

Map-based Channel Modeling and Generation for U2V mmWave Communication

Qiuming Zhu, *Member, IEEE*; Kai Mao; Maozhong Song; Xiaomin Chen, *Member, IEEE*; Boyu Hua; Weizhi Zhong, *Member, IEEE*; Xijuan Ye

Abstract—Unmanned aerial vehicle (UAV) aided millimeter wave (mmWave) technologies have a promising prospect in the future communication networks. By considering the factors of three-dimensional (3D) scattering space, 3D trajectory, and 3D antenna array, a non-stationary channel model for UAV-to-vehicle (U2V) mmWave communications is proposed. The computation and generation methods of channel parameters including inter-path and intra-path are analyzed in detail. The inter-path parameters are calculated in a deterministic way, while the parameters of intra-path rays are generated in a stochastic way. The statistical properties are obtained by using a Gaussian mixture model (GMM) on the massive ray tracing (RT) data. Then, a modified method of equal areas (MMEA) is developed to generate the random intra-path variables. Meanwhile, to reduce the complexity of RT method, the 3D propagation space is reconstructed based on the user-defined digital map. The simulated and analyzed results show that the proposed model and generation method can reproduce non-stationary U2V channels in accord with U2V scenarios. The generated statistical properties are consistent with the theoretical and measured ones as well.

Index Terms—U2V mmWave channel, channel model, channel generation, RT, statistical properties.

I. INTRODUCTION

UNMANNED aerial vehicles (UAVs) are expected to be an important part for the fifth and beyond fifth generation (5G/B5G) communication networks due to its flexible deployment, low cost, and high mobility [1], [2]. Moreover, the UAV-aided millimeter wave (mmWave) communication system can offer large capacity and good reliability due to its strong line-of-sight (LoS) connection link and wide bandwidth. However, compared with land mobile communication systems, the UAV-to-vehicle (U2V) communications also bring some challenges, i.e., three-dimensional (3D) scattering space, 3D trajectory, and 3D antenna array [3]–[5]. In order to efficiently design, optimize, and evaluate related communication technologies, it is vital to accurately model and reproduce the U2V mmWave channels [6], [7].

Channel models for UAV-aided communication systems at the sub-6GHz frequency band have been deeply studied during the past decade [8]–[12], but these models cannot be used at the mmWave band directly. Recently, several UAV mmWave channel models based on the geometry-based stochastic model (GBSM) can be addressed in [13]–[16]. For example, the authors in [13], [14] proposed a 3D GBSM for UAV mmWave channels which included the LoS, ground reflection, and single-bounce components. The authors in [15] proposed a 3D regular-shape GBSM for airborne-to-vehicle mmWave communications and analyzed the statistical properties of space-time-frequency correlation. The authors in [16] proposed a

3D GBSM for UAV-to-ground multiple-input multiple-output (MIMO) channels and it supported mmWave and massive MIMO configurations. Note that these stochastic models were easy to use but not well consistent with the user-defined specific scenarios. Certainly, field measurement based channel modeling is an accurate method to guarantee realistic channel characteristics for specific scenarios [17]–[21]. However, very few measurement campaigns have been performed for the mmWave band due to its high cost and difficult to implement [20], [21].

On the other hand, the ray tracing (RT) is a good alternative method to obtain accurate channel properties since the mmWave signal has quasi-optical characteristic. Recently, the RT-based channel modeling method has gained more and more attentions [22]–[25]. Some RT-based channel models can be addressed in [22], [23] and some propagation characteristics in different scenarios were analyzed in [24], [25]. Moreover, the standardized channel model such as METIS also supports a so-called map-based channel model by applying the RT technique on the pre-defined digital maps [26]. However, it should be mentioned that the RT method applying on the original digital map has high complexity and is extremely time-consuming. Meanwhile, it is impractical to trace and generate all rays due to the complexity of digital map. Thus, a hybrid model for terrestrial mobile channels was proposed by the 3GPP group [27], but it cannot be applied on the U2V scenarios with the rotation of UAVs. Moreover, the intra-cluster parameter generation method was based on the measurement results of terrestrial mobile systems. This paper aims to fill these research gaps. The main contributions and innovations are summarized as follows:

1) A non-stationary U2V mmWave channel model considering the new factors of 3D scattering space, 3D trajectories, and 3D antenna array is proposed. On this basis, a hybrid framework of channel generator for the pre-defined map is developed with a balance between the accuracy and complexity.

2) A map-based channel parameter computation and generation method is developed. The inter-path parameters are accurately calculated in a deterministic way based on the geometry relationships of specific digital map. The intra-path parameters are generated in a stochastic way. The statistical distributions are obtained by using a Gaussian mixture model (GMM) on the massive RT data in different scenarios. In order to speed up the RT process and reduce the complexity of parameter computation, a 3D reconstruction method for digital map is also given.

3) Based on the proposed model and generation method,

a typical UAV mmWave channel in the urban scenario is reproduced, analyzed, and validated. The statistical properties of generated channel, i.e., power delay profile (PDP), autocorrelation function (ACF), and Doppler power spectrum density (DPSD) are also validated by the theoretical and measured data.

The rest paper is organized as follows. In Section II, a 3D non-stationary channel model for U2V mmWave communications is proposed. Section III gives the computation and generation method of channel parameters. The simulation and validation of proposed model and generation method are given in Section IV. Finally, conclusions are drawn in Section V.

II. U2V MMWAVE CHANNEL GENERATION

A. U2V mmWave channel model

Let's consider a typical U2V communication scenario, where the UAV and vehicle are configured as the transmitter (TX) and receiver (RX) with their own velocities as

$$\mathbf{v}^{\text{tx/rx}}(t) = \left\| \mathbf{v}^{\text{tx/rx}} \right\| \begin{bmatrix} \cos \beta_v^{\text{tx/rx}}(t) \cos \alpha_v^{\text{tx/rx}}(t) \\ \cos \beta_v^{\text{tx/rx}}(t) \sin \alpha_v^{\text{tx/rx}}(t) \\ \sin \beta_v^{\text{tx/rx}}(t) \end{bmatrix} \quad (1)$$

where $\left\| \mathbf{v}^{\text{tx/rx}}(t) \right\|$ represents the velocity magnitude, $\alpha_v^{\text{tx/rx}}(t)$ and $\beta_v^{\text{tx/rx}}(t)$ represent the azimuth and elevation angles of velocity, respectively. The detailed parameters are listed in Table I.

According to the principle of radio propagation, the receiving signal can be expressed by the summation of N valid paths and each path including M_n rays with tiny delay difference [28]. For the 3D scattering space of U2V channels, the channel impulse response (CIR) should consider the impacts of signal propagation on both azimuth and elevation planes. Thus, the time-variant CIR of small scaling fading channel in this paper is modeled as

$$h(t, \tau, \Theta, \Phi) = \sum_{n=1}^N \sum_{m=1}^{M_n} \left\{ \sqrt{P_{n,m}} \tilde{A}_{n,m}(t) \delta(t - \tau_{n,m}(t)) \cdot \delta(\Theta - \Theta_{n,m}(t)) \delta(\Phi - \Phi_{n,m}(t)) \right\} \quad (2)$$

where the subscript $(\cdot)_{n,m}$ represents the m th ray within the n th path, $P_{n,m}(t)$, $\tau_{n,m}(t)$, $\tilde{A}_{n,m}(t)$ are the ray power, ray delay and complex ray coefficient, respectively. $\Theta_{n,m}(t) = (\alpha_{n,m}^{\text{tx}}(t), \beta_{n,m}^{\text{tx}}(t))$ and $\Phi_{n,m}(t) = (\alpha_{n,m}^{\text{rx}}(t), \beta_{n,m}^{\text{rx}}(t))$ are the angle of departure (AoD) and angle of arrival (AoA), where $\alpha_{n,m}^{\text{tx}}(t)$, $\beta_{n,m}^{\text{tx}}(t)$ denote the azimuth AoD (AAoD) and elevation AoD (EAoD), and $\alpha_{n,m}^{\text{rx}}(t)$, $\beta_{n,m}^{\text{rx}}(t)$ denote azimuth AoA (AAoA) and elevation AoA (EAoA).

For the 3D trajectory and 3D antenna array of U2V channels, the time-variant phase is much more complicated than terrestrial mobile channels. Two factors, i.e., Doppler effect phase caused by 3D trajectory and coordination rotation phase caused by non-linear movement and 3D-shaped array, are considered in this paper, and $\tilde{A}_{n,m}(t)$ can be expressed as

$$\tilde{A}_{n,m}(t) = \exp \left(\int_0^t j2\pi f_{n,m}(t') dt' + j\psi_{n,m}^{\text{R}}(t) + j\psi_{n,m}^{\text{I}} \right) \quad (3)$$

where $\psi_{n,m}^{\text{I}} = \int_{-\infty}^0 j2\pi f_{n,m}(t') dt' + \psi_{n,m}^{\text{I}}$ is a random phase with initial random phase $\psi_{n,m}^{\text{I}}$, $\psi_{n,m}^{\text{R}}(t)$ is the time-variant phase caused by rotation, and $f_{n,m}(t)$ is the Doppler frequency. In (3), $f_{n,m}(t)$ and $\psi_{n,m}^{\text{R}}(t)$ can be expressed respectively as

$$f_{n,m}(t) = \frac{f_0}{c} \left((\mathbf{v}^{\text{tx}}(t))^{\text{T}} \mathbf{r}_{n,m}^{\text{tx}}(t) + (\mathbf{v}^{\text{rx}}(t))^{\text{T}} \mathbf{r}_{n,m}^{\text{rx}}(t) \right) \quad (4)$$

$$\psi_{n,m}^{\text{R}}(t) = \frac{2\pi f_0}{c} \left(\mathbf{r}_{n,m}^{\text{rx}}(t) \cdot \mathbf{R}^{\text{rx}}(t) \cdot \mathbf{d}^{\text{rx}}(t) + \mathbf{r}_{n,m}^{\text{tx}}(t) \cdot \mathbf{R}^{\text{tx}}(t) \cdot \mathbf{d}^{\text{tx}}(t) \right) \quad (5)$$

where c is light speed, f_0 is the carrier frequency, $\mathbf{r}_{n,m}^{\text{tx/rx}}(t)$, $\mathbf{R}^{\text{tx/rx}}(t)$ and $\mathbf{d}^{\text{tx/rx}}(t)$ are the normalized direction vector, rotation matrix, and location vector, respectively. In (5), $\mathbf{r}_{n,m}^{\text{tx/rx}}(t)$ and $\mathbf{R}^{\text{tx/rx}}(t)$ can be further described as (6) and (7).

$$\mathbf{r}_{n,m}^{\text{tx/rx}}(t) = \begin{bmatrix} \cos \beta_{n,m}^{\text{tx/rx}}(t) \cos \alpha_{n,m}^{\text{tx/rx}}(t) \\ \cos \beta_{n,m}^{\text{tx/rx}}(t) \sin \alpha_{n,m}^{\text{tx/rx}}(t) \\ \sin \beta_{n,m}^{\text{tx/rx}}(t) \end{bmatrix} \quad (6)$$

B. Framework of channel generator

The proposed channel model has unique inter-path and intra-path characteristics due to high frequency with large bandwidth and high time resolution. The procedure of channel generation combining with RT method is shown in Fig. 1. Firstly, the inter-path parameters can be calculated based on the path tracing according to the geometric relationships. Secondly, massive data of intra-path ray parameters is obtained and used to extract the statistical distributions, i.e., delay offsets and angle offsets under different type scenarios. On this basis, the random ray parameters can be generated during each simulation. Finally, the U2V channels can be reproduced by combing the channel parameters with proposed model.

Considering that the realistic scenario contains abundant scatterers, the ray tracing process for the original map is extraordinarily complex and time-consuming. Thus, a reconstruction method is developed in this paper. Firstly, the digital terrain

TABLE I: Parameter definitions in the proposed model

Parameters	Definition
N	path number
M_n	intra-path ray number
$P_{n,m}(t), \tau_{n,m}(t)$	ray power and delay, respectively
M_n	path number
$\tilde{A}_{n,m}(t)$	ray complex coefficient
$\Theta_{n,m}(t), \Phi_{n,m}(t)$	AoD and AoA, respectively
$f_{n,m}(t)$	Doppler frequency
$\psi_{n,m}^{\text{I}}$	initial phase
$\psi_{n,m}^{\text{R}}(t)$	phase caused by antenna array rotation
$\mathbf{r}_{n,m}^{\text{tx/rx}}(t)$	normalized direction vector
$\mathbf{d}^{\text{tx/rx}}(t)$	location vector of TX (or RX)
$\mathbf{R}^{\text{tx/rx}}(t)$	rotation matrix of TX (or RX)

$$\mathbf{R}^{\text{tx/rx}}(t) = \begin{bmatrix} \cos \alpha_v^{\text{tx/rx}}(t) \cos \beta_v^{\text{tx/rx}} - \sin \alpha_v^{\text{tx/rx}} - \cos \alpha_v^{\text{tx/rx}} \sin \beta_v^{\text{tx/rx}} \\ \sin \alpha_v^{\text{tx/rx}} \cos \beta_v^{\text{tx/rx}} & \cos \alpha_v^{\text{tx/rx}} - \sin \alpha_v^{\text{tx/rx}} \sin \beta_v^{\text{tx/rx}} \\ \sin \beta_v^{\text{tx/rx}} & 0 & \cos \beta_v^{\text{tx/rx}} \end{bmatrix} \quad (7)$$

model (DEM) of user-defined scenario can be obtained from geographic database such as Google earth. The DEM file contains the information of latitude, longitude, and elevation of all points. These information is then used to reconstruct many regular or irregular triangle facets to approximately reconstruct the surface of 3D terrain and buildings.

III. CHANNEL PARAMETER COMPUTATION AND GENERATION

A. RT-based path parameter computation

The mmWave signal propagation process has apparent quasi-optical characteristic. Based on the ray optics and uniform theory of diffraction theory, the RT method can precisely analyze the mmWave propagation process with a specific map. The proposed RT-based parameter computation method includes three steps, i.e., decomposition of ray source, tracking of rays, and superposition of field strength. Since it is impossible to

track all the rays from the signal source, we choose the rays uniformly distributed on the sphere. The azimuth and elevation angles of candidate rays can be expressed respectively as

$$\begin{aligned} \varphi &= i\delta, i = 1 \cdots \text{int}(180/\delta) \\ \theta &= j\delta/\sin(\varphi), j = 1 \cdots \text{int}(360 \sin(\varphi)/\delta) \end{aligned} \quad (8)$$

where δ denotes the angle space, $\text{int}(\cdot)$ means the integer part. In order to track the full propagation trace of candidate rays, it's important to find the reflected point that the rays hit. Since each reconstructed scatterer consists of several triangle facet, we denote the target triangle facet as $V_0V_1V_2$ and the location vector of V_0, V_1, V_2 are denoted as $\mathbf{V}_0, \mathbf{V}_1$ and \mathbf{V}_2 , respectively. The location vector \mathbf{P} of arbitrary point P in triangle facet can be expressed as

$$\mathbf{P} = p_0\mathbf{V}_0 + p_1\mathbf{V}_1 + p_2\mathbf{V}_2 \quad (9)$$

where p_0, p_1, p_2 can be further determined by

$$\begin{cases} p_0 + p_1 + p_2 = 1 \\ p_0 = \frac{S(PV_1V_2)}{S(V_0V_1V_2)}, p_0 \in [0, 1] \\ p_1 = \frac{S(PV_0V_2)}{S(V_0V_1V_2)}, p_1 \in [0, 1] \\ p_2 = \frac{S(PV_0V_1)}{S(V_0V_1V_2)}, p_2 \in [0, 1] \end{cases} \quad (10)$$

where $S(\cdot)$ is the triangle area. Let us denote the location of signal source as \mathbf{Q} , then the location of each point along the i th ray can be expressed as

$$\mathbf{I}_i = \mathbf{Q} + w_1\mathbf{S}_i \quad (11)$$

where w_1 is the length, \mathbf{S}_i is the spherical unit vector and can be expressed as

$$\mathbf{S}_i = [\sin \varphi \cos \theta \quad \sin \varphi \sin \theta \quad -\cos \varphi]^T. \quad (12)$$

By using the Snell's law, the unit vector of i th reflected ray can be expressed as \mathbf{P}_i is a possible reflected point, it can be determined by

$$\mathbf{S}_i^{\text{Ref}} = \mathbf{S}_i - 2(\mathbf{S}_i \cdot \mathbf{k})\mathbf{k} \quad (13)$$

where \mathbf{k} is the unit vector of triangle facet. Assuming that \mathbf{P}_i is a possible reflected point, it can be determined by

$$\begin{cases} \mathbf{P}_i = \mathbf{I}_i \\ \mathbf{P}_i = \mathbf{R} - \|\mathbf{P}_i - \mathbf{R}\|_2 \mathbf{S}_i^{\text{Ref}}, \mathbf{P}_i \in \mathbf{P} \end{cases} \quad (14)$$

where w_2 is the ray length from the reflected point to the RX, and \mathbf{R} is the location vector of RX.

The arrival rays at the RX usually include two cases, e.g., direction and reflection. For the direct case, the electric field intensity can be calculated by

$$\mathbf{E}^{\text{LoS}}(t) = \mathbf{E}^{\text{1m}} \frac{e^{-jtd_0^{\text{tx}}(t)}}{d_0^{\text{tx}}(t)} \quad (15)$$

where \mathbf{E}^{1m} is the electric field intensity of 1 m from the TX,

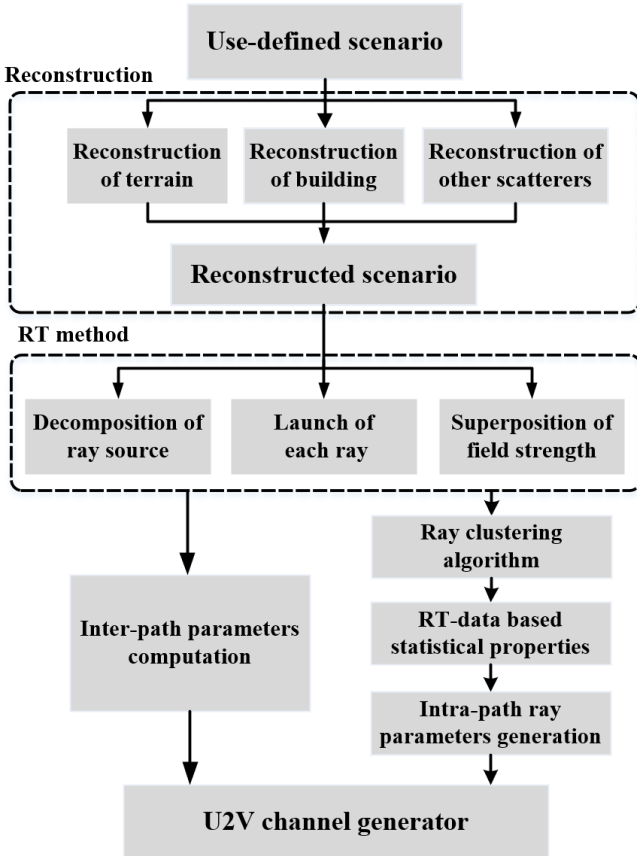


Fig. 1. Procedure of channel generation.

$$\bar{\alpha}_n^{\text{rx}}(t) = \begin{cases} \arccos\left(\frac{|\bar{\mathbf{P}}_n^x - \mathbf{R}^x|}{\sqrt{|\bar{\mathbf{P}}_n^x - \mathbf{R}^x|^2 + |\bar{\mathbf{P}}_n^y - \mathbf{R}^y|^2}}\right), \bar{\mathbf{P}}_n^x - \mathbf{R}^x \geq 0 \\ \pi - \arccos\left(\frac{|\bar{\mathbf{P}}_n^x - \mathbf{R}^x|}{\sqrt{|\bar{\mathbf{P}}_n^x - \mathbf{R}^x|^2 + |\bar{\mathbf{P}}_n^y - \mathbf{R}^y|^2}}\right), \bar{\mathbf{P}}_n^x - \mathbf{R}^x < 0 \end{cases} \quad (20)$$

$l = 1/\lambda_0$ is the wave number, and $d_0^{\text{tx}}(t) = \|\mathbf{Q} - \mathbf{R}\|_2$ is the distance between the UAV and RX. For the reflected case, it can be obtained by

$$\mathbf{E}_m^{\text{R}}(t) = \mathbf{E}^{\text{lm}} R \frac{e^{-lj(d_m^{\text{tx},\text{S}}(t) + d_m^{\text{S},\text{rx}}(t))}}{d_m^{\text{tx},\text{S}}(t) + d_m^{\text{S},\text{rx}}(t)} \quad (16)$$

where R is the reflection coefficient, $d_m^{\text{tx},\text{S}}(t) = \|\mathbf{Q} - \mathbf{P}_i\|_2$ is the distance between the UAV and the scatterer, and $d_m^{\text{S},\text{rx}}(t) = \|\mathbf{P}_i - \mathbf{R}\|_2$ is the distance between the RX and scatterer. Finally, the power gain of m th ray can be obtained by

$$P_m = 10 \log_{10} \left(G^{\text{rx}} G^{\text{tx}} \left(\frac{\lambda_0}{4\pi} \right)^2 \left| \frac{\mathbf{E}_m^{\text{R}}}{\mathbf{E}_{1\text{m}}} \right| \right) \quad (17)$$

where G^{tx} and G^{rx} are antenna gains of TX and RX, respectively. The power gain of direction ray can be calculated similarly.

Note that each non-light-of-sight (NLoS) path contains several intra-path rays and the arrival rays from the same scatterer have similar delays. In this paper, the ray delays within each path are modeled by adding an intra-path delay offset $\Delta\tau_{n,m}$ on the mean path delay $\bar{\tau}_n(t)$ as

$$\tau_{n,m}(t) = \bar{\tau}_n(t) + \Delta\tau_{n,m}. \quad (18)$$

Similarly, the ray angles $\alpha_{n,m}^{\text{rx}}(t)$, $\beta_{n,m}^{\text{rx}}(t)$ can be modeled as several intra-path offsets $\Delta\alpha_{n,m}$, $\Delta\beta_{n,m}$ deviating from the mean path angle $\bar{\alpha}_n^{\text{rx}}(t)$, $\bar{\beta}_n^{\text{rx}}(t)$, which have similar models as (18).

In this paper, the inter-path delays and angles are calculated in a deterministic way. The adjacent reflection points are assumed to be one centroid and the location vector is denoted as $\bar{\mathbf{P}}_n$. The mean values of path delay, AAoA, and EAoA can be expressed respectively as (19),(20) and (21).

$$\bar{\tau}_n(t) = \frac{\|\mathbf{Q} - \bar{\mathbf{P}}_n\|_2 + \|\bar{\mathbf{P}}_n - \mathbf{R}\|_2}{c} \quad (19)$$

$$\bar{\beta}_n^{\text{rx}}(t) = \arcsin \left(\frac{|\bar{\mathbf{P}}_n^z - \mathbf{R}^z|}{\|\bar{\mathbf{P}}_n - \mathbf{R}\|_2} \right) \quad (21)$$

where $(\cdot)^x$, $(\cdot)^y$ and $(\cdot)^z$ represent the x, y, and z component, respectively. Similarly, the mean path power $\bar{P}_n(t)$ can be calculated by (15)–(17).

B. RT-statistical parameters and generation

There is no need to calculate all ray parameters in each channel modeling or generation for three reasons. Firstly, each scenario includes numerous scatterer elements, e.g., vegetation, puddles, roads, and different roof structures, which may result in several hours of computation time. Secondly, it is impossible to describe the realistic propagation scenario perfectly. For example, the material of composite scatterers, irregular building

surface, branches and leaves of trees are difficult to describe. Thirdly, there are lots of scatterers such as trains, vehicles, and pedestrian that are usually in motion and do not have fixed positions. In the proposed generator, the ray parameters are generated in a stochastic way based on the empirical statistical properties.

In order to obtain the statistical properties of intra-path ray parameters, four typical realistic scenarios included in most of standardized channel models, i.e., urban, hilly, forest, and sea, are studied in this section. We set 50 ground RXs at the height of 2 m and 500 UAV-based TXs at the height of 150 m in each scenario. By applying the RT method, the U2V channels between 25000 pairs of transceivers are obtained in different scenarios, where each channel contains massive propagation rays. Furthermore, the ray parameters, i.e., delays, angles and powers, are analyzed to get the statistical properties of intra-path ray offsets. The acquisition RT-based data under urban scenario is shown in Fig. 2.

To further analyze the intra-path ray parameters, the key step is to group the rays into several clusters with similar characteristics, e.g., delay and AoA. Here, the distance between two rays is defined by the multiple component distance (MCD) as (22).

On this basis, $\text{MCD}_\tau(m_i, m_j)$ and $\text{MCD}_{\text{AoA}}(m_i, m_j)$ can be obtained respectively by (23) and (24).

$$\text{MCD}_\tau(m_i, m_j) = \zeta \frac{|\tau_{m_i} - \tau_{m_j}| \tau_{std}}{\Delta\tau_{\text{max}}^2} \quad (23)$$

where ζ is the delay factor, τ_{m_i/m_j} is the ray delay, τ_{std} is the standard deviation of ray delays, and $\Delta\tau_{\text{max}}$ is the maximum value of relative delays. In (24), α_{m_i/m_j} and β_{m_i/m_j} represent the AAoA and EAoA, respectively. When the MCD of two rays is smaller than the threshold MCD_{thr} , they would be grouped into the same cluster. Algorithm 1 gives the procedure of our new clustering method, where

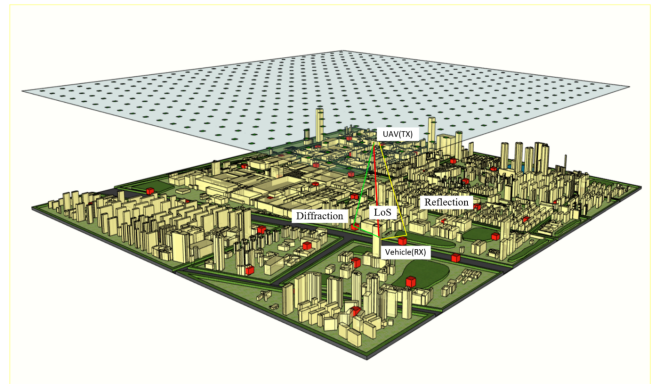


Fig. 2. Acquisition of massive RT-based data.

$$\text{MCD}(m_i, m_j) = \sqrt{\|\text{MCD}_\tau(m_i, m_j)\|^2 + \|\text{MCD}_{\text{AoA}}(m_i, m_j)\|^2} \quad (22)$$

$$\text{MCD}_{\text{AoA}}(m_i, m_j) = \frac{1}{2} \left\| \begin{bmatrix} \sin \beta_{m_i} \cos \alpha_{m_i} \\ \sin \beta_{m_i} \sin \alpha_{m_i} \\ -\cos \beta_{m_i} \end{bmatrix} - \begin{bmatrix} \sin \beta_{m_j} \cos \alpha_{m_j} \\ \sin \beta_{m_j} \sin \alpha_{m_j} \\ -\cos \beta_{m_j} \end{bmatrix} \right\|_2 \quad (24)$$

$X_m = \{P_m, \tau_m, \alpha_m, \beta_m | m = 1, 2, \dots, M\}$ is the aggregate containing all the rays and X_n is the aggregate containing the rays within the n th path.

Algorithm 1: Ray clustering method

Input: Aggregate X_m ;

Output: Aggregate X_n ;

- 1: **Initialize** $N = 0, n = 1, \zeta = 3, \tau_{std} = \text{std}(\tau_m)$;
- 2: $\Delta\tau_{\max} = \max\{|\tau_{m_i} - \tau_{m_j}|\}, \tau_{m_i}, \tau_{m_j} \in \mathbf{X}_m$;
- 3: **while** $X_m \not\subseteq \emptyset$ **do**
- 4: $k = \text{find}(P_m == \max(P_m)), P_m \in \mathbf{X}_m$;
- 5: **for** $m = 1 : \text{card}(X_m)$ **do**
- 6: **if** $\text{MCD}(m, k) \leq \text{MCD}_{thr}$ **then**
- 7: $X_m = X_m - \{P_m, \tau_m, \alpha_m, \beta_m\}$;
- 8: $X_n = X_n + \{P_m, \tau_m, \alpha_m, \beta_m\}$;
- 9: **end if**
- 10: **end for**
- 11: $n = n + 1$;

By applying the ray clustering method on massive channel data, huge amount of output X_n is analyzed to get the statistical properties of ray parameters under different scenarios. The delay offset of rays deviating from the mean path delay are shown in Fig. 3. As a general and classic distribution, the Gaussian distribution (GD) is previously used to fit the distribution of channel parameters [27]. However, we have found that GD cannot fit well with the PDF of ray delay offset. Instead, a Gaussian mixture model (GMM) is adopted in this paper. As we can see in Fig. 3, the GMM fits better than the traditional GD. To further evaluate the goodness of fit, the root mean square errors (RSMES) of GMM and GD are calculated by

$$R_e = \sqrt{\frac{1}{K} \sum_{k=1}^K (y_k - \hat{y}_k)^2} \quad (25)$$

where y_k, \hat{y}_k represent the PDF of RT data and fitted data, respectively. In Fig. 3, R_e of GMM are 0.0021, 0.0052, 0.009, 0.001 under four scenarios, which outperform the 0.0317, 0.0341, 0.0195, 0.021 of GD. For this reason, the ray delay offset is modeled as

$$f_{\Delta\tau}(\tau) = \sum_{i=1}^I \frac{a_i}{\sqrt{2\pi}\sigma_i} \exp\left(-\frac{(\tau - \mu_i)^2}{2\sigma_i^2}\right) \quad (26)$$

where I is 2 in this paper, a_i is the weight factor of the magnitude, μ_i is the mean value and σ_i is the standard deviation. The fitting parameters of $a_1, \mu_1, \sigma_1, a_2, \mu_2$ and σ_2 are listed in Table II.

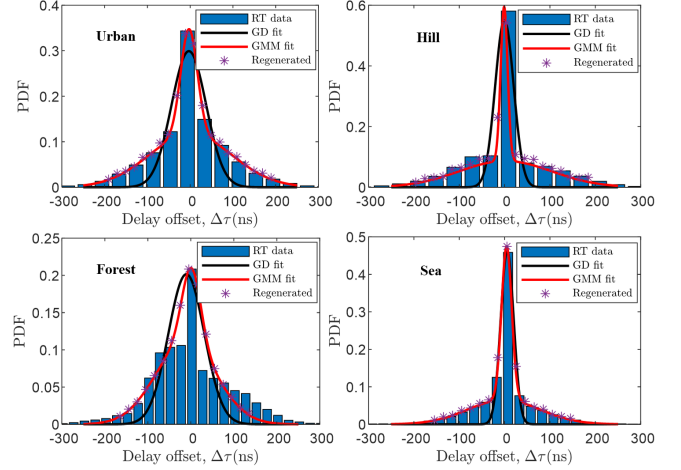


Fig. 3. PDFs of ray delay offset.

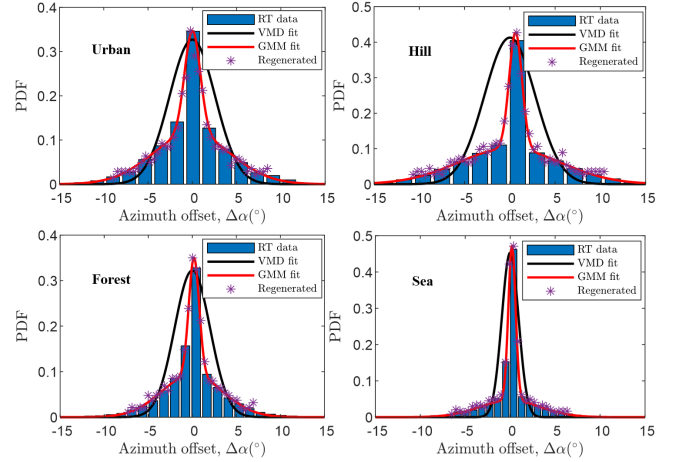


Fig. 4. The PDFs of azimuth offset.

On the other hand, the Von Mises distribution (VMD) is widely used to describe the distribution of AoA and AoD [29]. However, we also find that the PDFs of azimuth and elevation angle offset can be fitted better by the GMM as shown in Fig. 4 and Fig. 5. In Fig. 4, R_e of GMM are 0.0028, 0.0009, 0.0024, 0.0022 under four scenarios, which outperform the 0.0301, 0.0505, 0.0274, 0.0401 of VMD. In Fig. 5, R_e of GMM are 0.0023, 0.0018, 0.0014, 0.0013, which outperform the 0.0115, 0.0170, 0.0220, 0.0163 of VMD. The fitting parameters of the PDFs of azimuth and elevation angle offset are also listed in Table II.

For providing random ray parameters for each channel generation, we adopt a MMEA method to generate the random variables based on the above GMM distributions. Taking the ray delay offset as an example, the MMEA can be expressed

TABLE II: Fitting parameters of PDFs

Scenarios		Urban	Hilly	Forest	Sea
Delay offset	a_1	11.244	9.751	5.577	11.522
	μ_1	-2.747	-1.090	1.391	4.438
	σ_1	19.410	7.644	21.748	11.201
	a_2	56.199	22.170	19.373	12.998
	μ_2	0.903	1.761	-11.780	-1.332
	σ_2	97.015	102.248	70.711	80.186
Azimuth offset	a_1	0.519	0.584	0.379	0.432
	μ_1	0.013	0.630	0.191	0.201
	σ_1	0.886	0.712	0.588	0.404
	a_2	1.259	1.431	0.809	0.394
	μ_2	-0.083	-0.054	-0.015	-0.004
	σ_2	4.431	5.685	3.471	3.386
Elevation offset	a_1	0.371	0.984	0.642	0.629
	μ_1	-0.131	0.244	0.167	0.069
	σ_1	0.565	0.699	0.437	0.354
	a_2	0.476	0.345	0.162	0.138
	μ_2	0.027	-1.345	-1.323	-0.107
	σ_2	2.210	4.295	5.046	2.303

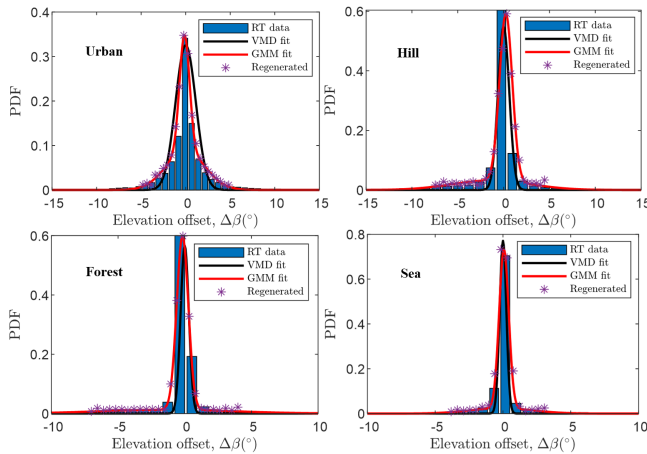


Fig. 5. The PDFs of elevation offset.

as

$$\int_{\tau_{k-1}}^{\tau_k} f_{\Delta\tau}(\tau) d\tau = \frac{1}{K}, k = 1, 2, \dots, K \quad (27)$$

where the initial value of τ_0 is determined by the distribution range of GMM and K is the total number of required parameters. Note that there is no closed-form expression of GMM integration. In this paper, the integral interval is divided into I small parts and the equation (27) can be equivalently rewritten as

$$\sum_{i=0}^{I-1} f\left(\frac{i\tau_k + (I-i)\tau_{k-1}}{I}\right) \frac{\tau_k - \tau_{k-1}}{I} = \frac{1}{K} \quad (28)$$

To verify the effectiveness of MMEA method, we perform this method to generate 100000 samples of each kind of parameters under four scenarios. The statistical distributions of generated data are plotted with the fitting curve in Fig. 3 – Fig. 5 for comparison purpose. As we can see that the PDFs of regenerated data are consistent with previous obtained GMM fitting curves under four scenarios. In previous work, we have found that the power in dB can be expressed as a

linear expression with respect to the delay within each path [14]. So, the ray power offset can be calculated by

$$\Delta P_{n,m} = \log_{10}(e)\zeta\Delta\tau_{n,m} \quad (29)$$

where ζ is a linear slope that depends on the scenarios. Finally, the channel parameter of ray power can be obtained by

$$P_{n,m}(t) = \bar{P}_n(t) + \Delta P_{n,m}. \quad (30)$$

IV. SIMULATION RESULTS AND ANALYZE

To verify the correctness of proposed channel model, the UAV mmWave channels under a typical urban scenario are simulated at 28 GHz. The satellite view and reconstructed digital map of simulation scenario are shown in Fig. 4. The UAV flies at the constant height of 150 m with the velocity of 10 m/s. In the urban scenario, the buildings with average height of 30 m are densely distributed and the main material of buildings are concrete. Moreover, the soil moisture of the scenarios is considered as well. The proposed U2V mmWave channel model at 28 GHz under the urban scenario is generated and validated in this section. The satellite view and reconstructed scenario for channel generation are shown in Fig. 6. The UAV flies at the constant height of 150 m with the velocity of 10 m/s and the ground Rx moves with the velocity of 1 m/s. Both of the UAV and Rx are equipped with omnidirectional antennas. For the undergoing urban scenario, the buildings with average height of 30 m are densely distributed and the main material of buildings are assumed to be concrete.

The time-variant 3D PDPs of generated channel along the flight trajectory is given in Fig. 7. The absolute time delay is used to directly show the delay varying along with the movement of UAV. In Fig. 7, we can find that when the distance between UAV and ground receiver is shorter, the path delay is smaller and the power is bigger, and vice versa. Moreover, it can be seen that the LoS path only exists between about 80 s and 180 s due to the obstacle of high buildings. There is an NLoS path closely near the LoS path which is the ground reflected path. Moreover, some other NLoS paths appear or disappear in different time instant, which also demonstrate the birth-and-death process of propagation paths in UAV communications [10].

The second order statistical properties, i.e., ACF and DPSD, are often used to evaluate the effectiveness of channel models. The normalized ACF can be expressed as

$$r(t; \Delta t) = \frac{E[h^*(t)h(t + \Delta t)]}{\sqrt{E[|h^*(t)|^2] E[|h(t + \Delta t)|^2]}} \quad (31)$$

where $E(\cdot)$ is the expectation function and $(\cdot)^*$ is the complex conjugate. The DPSD can be obtained by the Fourier transform on ACF. The time-variant DPSD of proposed channel generation method is given in Fig. 8(a). It can be seen that when the UAV flies over the receiver, the Doppler frequency of LoS path rapidly turns into negative after 150 s. The Doppler frequencies of NLoS paths are complicated due to the 3D scattering environment and 3D trajectory of UAV communication scenario. For comparison purpose, based on the full RT method on

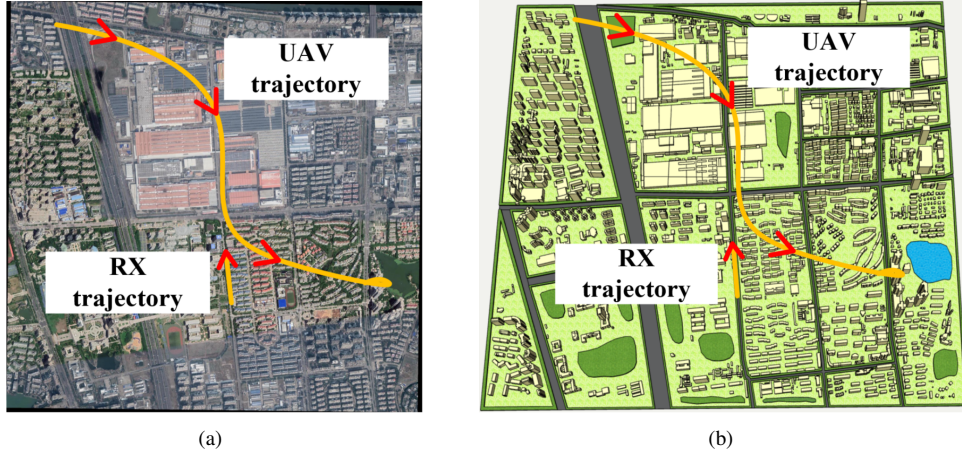


Fig. 6. (a) Satellite view and (b) reconstructed urban scenario.

the reconstructed urban scenario, the calculated DPSD is also shown in Fig. 8(b). Due to randomness of parameter generation, the calculated result can only be qualitatively compared with the generated one. It shows that the DPSD of proposed method has the same trend with the ones of RT simulation. To further verify the consistency of proposed method with the realistic channel, the ACF is simulated in the similar scenario as [30] at 24 GHz, and the comparison results in Fig. 9 show that the ACF of proposed channel generator is consistent with the measured one.

V. CONCLUSIONS

This paper has proposed a non-stationary 3D U2V mmWave channel model considering 3D scattering, 3D trajectory, and 3D antenna array. Meanwhile, a map-based parameter computation and generation method has been developed, which could guarantee both the efficiency and precision. The inter-path parameters have been accurately calculated in a deterministic way based on the geometric parameters. The intra-path parameters have been generated by the fitting GMM according to the massive channel data. Moreover, a simplified map reconstruction method has also given to reduce the complexity of channel generation. At last, the statistical properties of proposed channel model, i.e., PDP, ACF, and DPSD, have been generated and verified

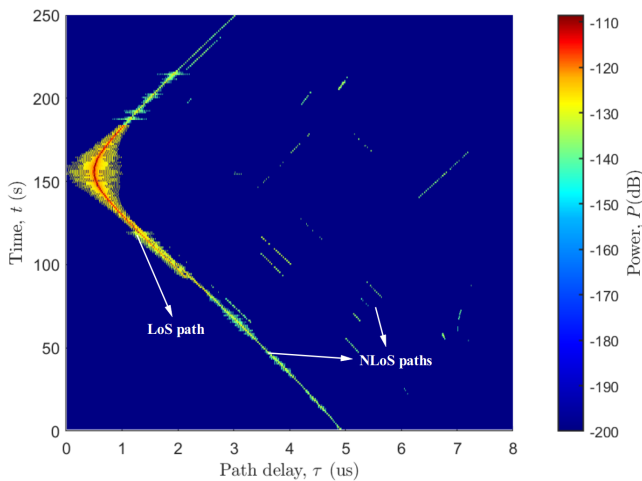


Fig. 7. The generated time-variant PDPs.

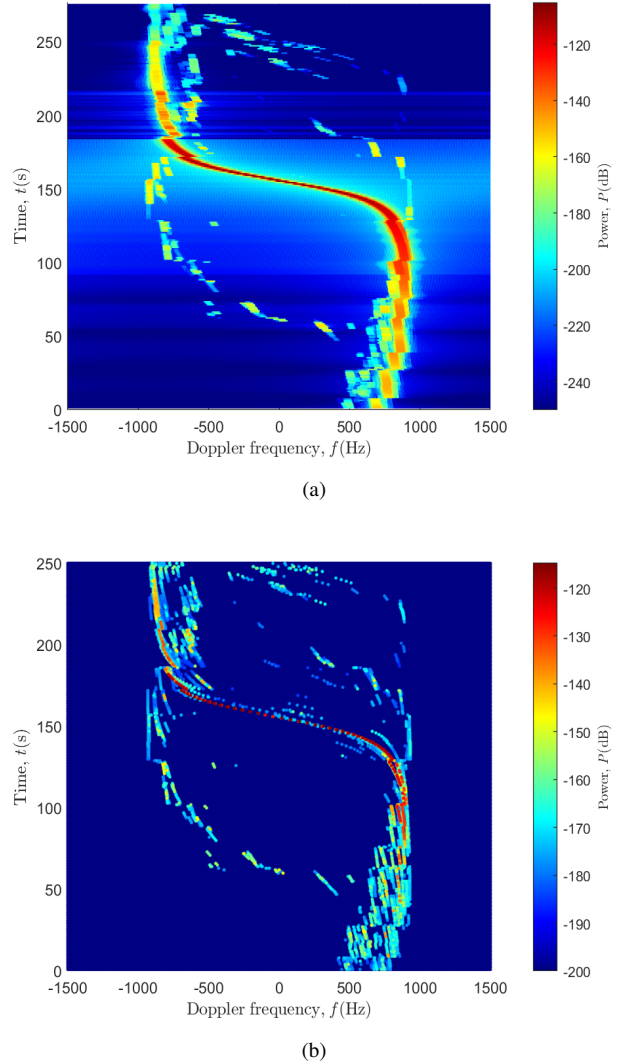


Fig. 8. The time-variant DPSDs of (a) proposed channel generator and (b) deterministic RT method.

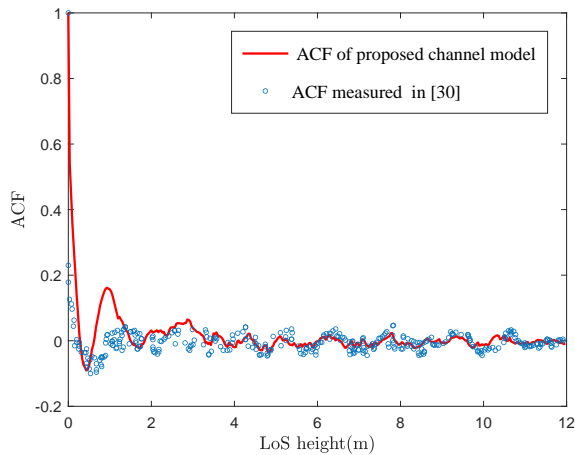


Fig. 9. The generated and measured ACFs.

with the calculated and measured results. In the future, we will perform channel measurements to optimize the intra-path parameters as well as the channel model.

REFERENCES

- [1] L. Bin, F. Zesong, and Z. Yan, "UAV communications for 5G and beyond: recent advances and future trends," *IEEE Internet Things J.*, vol. 6, no. 2, pp. 2241–2263, Dec. 2018.
- [2] C.-X. Wang, and M. C. Gursoy, "Coverage analysis for energy-harvesting UAV assisted mmWave cellular networks," *IEEE Journ. Sel. Areas Commun.*, vol. 37, no. 12, pp. 2832–2850, Dec. 2019.
- [3] W. Khawaja, I. Guvenc, D. W. Matolak, U. Fiebig, and N. Schneckenburger, "A survey of air-to-ground propagation channel modeling for unmanned aerial vehicles," *IEEE Commun. Surv. & Tuts.*, vol. 21, no. 3, pp. 2361–2391, May. 2019.
- [4] C. Zhang, W. Zhang, W. Wang, L. Yang, and W. Zhang, "Research challenges and opportunities of UAV millimeter-wave communications," *IEEE Wireless Commun.*, vol. 26, no. 1, pp. 58–62, Feb. 2019.
- [5] W. Zhong, L. Xu, Q. Zhu, X. Chen, and J. Zhou, "MmWave beamforming for UAV communications with unstable beam pointing," *China Commun.*, vol. 16, no. 1, pp. 37–46, Jan. 2019.
- [6] Z. Ullah, F. Al-Turjman, and L. Mostarda, "Cognition in UAV-aided 5G and beyond communications: a survey," *IEEE Trans. Cognitive Commun. & Networking*, vol. 6, no. 3, pp. 827–891, Sep. 2020.
- [7] X. Chen, X. Hu, Q. Zhu, W. Zhong, and B. Chen, "Channel modeling and performance analysis for UAV relay systems," *China Commun.*, vol. 15, no. 12, pp. 89–97, Sep. 2018.
- [8] H. Chang, J. Bian, C.-X. Wang, and E. M. Aggoune, "A 3D non-stationary wideband GBSM for low-altitude UAV-to-ground V2V MIMO channels," *IEEE Access*, vol. 13, no. 16, pp. 2617–2627, Oct. 2019.
- [9] X. Zhang, and X. Cheng, "Three-dimensional non-stationary geometry-based stochastic model for UAV-MIMO Ricean fading channels," *IET Commun.*, vol. 13, no. 16, pp. 2617–2627, Oct. 2019.
- [10] Q. Zhu, K. Jiang, X. Chen, W. Zhong, and Y. Yang, "A novel 3D non-stationary UAV-MIMO channel model and its statistical properties," *China Commun.*, vol. 15, no. 12, pp. 147–158, Dec. 2018.
- [11] C. Yan, L. Fu, J. Zhang, and J. Wang, "A comprehensive survey on UAV communication channel modeling," *IEEE Access*, vol. 7, pp. 107769–107792, Aug. 2019.
- [12] Cui Z, Guan K, Briso-Rodriguez C, Ai B, and Zhong Z, "Towards connected unmanned aerial system: a channel modeling perspective," *arXiv preprint*, vol. 2012, pp. 6707, Dec. 2020.
- [13] Q. Zhu, Y. Wang, K. Jiang, X. Chen, W. Zhong, and N. Ahmed, "3D nonstationary geometry-based multi-input multi-output channel model for UAV-ground communication systems," *IET Microw., & Antennas Propag.*, vol. 8, no. 13, pp. 1104–1112, Apr. 2019.
- [14] Mao K, Zhu Q, Song M, Hua B, Zhong W, and Ye X, "A geometry-based beamforming channel model for UAV mmWave communications," *Sensors*, vol. 20, no. 23, pp. 6957–6973, Dec. 2020.
- [15] E. T. Michailidis, N. Nomikos, P. Trakadas, and A. G. Kanatas, "Three-dimensional modeling of mmWave doubly massive MIMO aerial fading channels," *IEEE Trans. Vehi. Tech.*, vol. 69, no. 2, pp. 1190–1202, Feb. 2020.
- [16] H. Chang, C. Wang, Y. Liu, J. Huang, J. Sun, et al., "A novel non-stationary 6G UAV-to-ground wireless channel model with 3D arbitrary trajectory changes," *IEEE Internet Things J.*, Aug. 2020, doi: 10.1109/IJOT.2020.3018479.
- [17] X. Cai, R. Jose, X. Yin, N. Wang, B. Ai, et al., "An empirical air-to-ground channel model based on passive measurements in LTE," *IEEE Trans. Vehi. Tech.*, vol. 68, no. 2, pp. 1140–1154, Feb. 2019.
- [18] Z. Yang, L. Zhou, G. Zhao, and S. Zhou, "Channel model in the urban environment for unmanned aerial vehicle communications," in *proc. EuCAP'18*, London, UK, Apr. 2018, pp. 1–5.
- [19] Matolak D W, and Sun R, "Air-ground channel characterization for unmanned aircraft systems–Part III: The suburban and near-urban environments," *IEEE Trans. Vehi. Tech.*, vol. 66, no. 8, pp. 6607–6618, Aug. 2017.
- [20] W. Khawaja, O. Ozdemir, and I. Guvenc, "UAV air-to-ground channel characterization for mmWave systems," in *Proc. VTC'17*, Toronto, ON, Sep. 2017, pp. 1–5.
- [21] R. Geise, A. Weiss, and B. Neubauer, "Modulating features of field measurements with a UAV at millimeter wave frequencies," in *Proc. CAMA'18*, Vasteras, Sweden, Sep. 2018, pp. 1–4.
- [22] L. Cheng, Q. Zhu, C. Wang, W. Zhong, B. Hua, et al., "Modeling and simulation for UAV air-to-ground mmWave channels," in *Proc. EuCAP'20*, Copenhagen, Denmark, Mar. 2020, pp. 1–5.
- [23] W. Khawaja, O. Ozdemir, and I. Guvenc, "Temporal and spatial characteristics of mm Wave propagation channels for UAVs," in *proc. GSSM'18*, Boulder, CO, USA, May. 2018, pp. 1–6.
- [24] G. Yang, Y. Zhang, Z. He, J. Wen, Z. Ji, and Y. Li, "Machine-learning-based prediction methods for path loss and delay spread in air-to-ground millimetre-wave channels," *IEEE Trans. Microw., Antennas & Propag.*, vol. 13, no. 8, pp. 1113–1121, June 2019.
- [25] P. Alberto, A. Fouda, and A. S. Ibrahim, "Ray tracing analysis for UAV-assisted integrated access and backhaul millimeter wave networks," in *Proc. WoWMoM'19*, Washington, DC, USA, Aug. 2019, pp. 1–5.
- [26] ICT-317669 METIS Project deliverable D1.4 v.3, *METIS Channel Models*, June 2015.
- [27] 3GPP TR 38.901 V15.0.0, Study on channel model for frequencies from 0.5 to 100 GHz, June 2018.
- [28] Q. Zhu, S. Jiang, C. X. Wang, B. Hua, K. Mao, et al., "Effects of digital map on the RT-based channel model for UAV mmWave communications," in *Proc. IWCMC'20*, Limassol, Cyprus, June 2020, pp. 1648–1653.
- [29] Z. Ma, B. Ai, R. He, G. Wang, Y. Niu, et al. "A wideband non-stationary air-to-air channel model for UAV communications," *IEEE Trans. Vehic. Technol.*, vol. 69, no. 2, pp. 1214–1226, Feb. 2020.
- [30] Z. Cui, C. Briso-Rodriguez, K. Guan, Z. Zhong, and F. Quitin, "Multi-frequency air-to-ground channel measurements and analysis for UAV communication systems," *IEEE Access*, vol. 8, pp. 110565–110574, June 2020.